
LIGHTWEIGHT TRANSFORMERS FOR HUMAN ACTIVITY RECOGNITION ON MOBILE DEVICES

Sannara EK
sannara.ek@univ-grenoble-alpes.fr
University Grenoble Alpes
LIG F-38000
Grenoble, France

François PORTET
francois.portet@imag.fr
University Grenoble Alpes
LIG F-38000
Grenoble, France

Philippe LALANDA
philippe.lalanda@imag.fr
University Grenoble Alpes
LIG F-38000
Grenoble, France

ABSTRACT

Human Activity Recognition (HAR) on mobile devices has shown to be achievable with lightweight neural models learned from data generated by the user's inertial measurement units (IMUs). Most approaches for instance-based HAR have used Convolutional Neural Networks (CNNs), Long Short-Term Memory (LSTMs), or a combination of the two to achieve state-of-the-art results with real-time performances. Recently, the Transformers architecture in the language processing domain and then in the vision domain has pushed further the state-of-the-art over classical architectures. However, such Transformers architecture is heavyweight in computing resources, which is not well suited for embedded applications of HAR that can be found in the pervasive computing domain. In this study, we present Human Activity Recognition Transformer (HART), a lightweight, sensor-wise transformer architecture that has been specifically adapted to the domain of the IMUs embedded on mobile devices. Our experiments on HAR tasks with several publicly available datasets show that HART uses fewer Floating-point Operations Per Second (FLOPS) and parameters while outperforming current state-of-the-art results. Furthermore, we present evaluations across various architectures on their performances in heterogeneous environments and show that our models can better generalize on different sensing devices or on-body positions.

Keywords Human Activity Recognition, Mobile Sensing, Lite-weight AI, Transformers

1 Introduction

Pervasive computing promotes the integration of smart electronic devices in our living and working spaces in order to provide a wide variety of services. This concept, which has been around for many years now [1, 2], is becoming increasingly popular and is now being applied in many areas. This is due in particular to the appearance of ever more varied and precise devices in our environments, which make it possible to implement quality services with high added value. This is also due to advances in software engineering to handle dynamic and stochastic environments, as well as the use of recent machine learning techniques. The goal of machine learning is to train algorithms to automatically make a decision by identifying patterns that may be hidden within massive data sets and, therefore, cannot be programmed explicitly. ML techniques are particularly suitable for pervasive systems where traditional solutions cannot be used because of the lack of modeling tools and excessive algorithmic complexity.

The field of wearable devices is particularly representative of recent developments. Smartphones or smartwatches, for instance, are equipped with many high-quality Inertial Measuring Units (IMU) sensors, like accelerometer and gyroscope, that opens the way to a number of health, wellness, or simply informational services [3]. These devices have thus become essential elements for the provision of personal services. In particular, wearable devices are used today to identify and monitor a person's basic activities automatically. This feature is usually referred to as "Human Activity Recognition" (HAR) and includes recognition of movements such as walking, jumping, climbing or descending, or maintaining a standing, sitting, or lying position. Such movement detection is the basic building block for identifying and tracking more complex activities, which requires introducing a broader context of execution [4].

Most solutions to recognize basic human movements are based on deep learning techniques that make use of the continuous streams of data provided by the worn sensors. Precisely, many studies on instanced-based HAR have employed Convolutional Neural Networks (CNNs), Long Short-Term Memory (LSTMs), or a combination of the two to achieve state-of-the-art results [5, 6]. Those approaches have demonstrated high recognition rates reaching 90% or more. However, deploying HAR systems in real-world environments is still challenging to achieve mainly due to poor data distribution, the lack of well-labeled data, the lack of standard benchmarks, and the difficulty dealing with heterogeneous matters and environments.

In this work, we focus on the heterogeneity problem with compliance to the constraint of low-resourced mobile devices. Permitting unmoderated usage by the clients tends to lead the trained model to underperform and is an open challenge for any ML-based approach. The cause is known to be due to statistical heterogeneity (difference between client data caused by differences in individual user’s usage and environment) and system heterogeneity (difference between client data caused by different system traits) which causes dissimilarity between the inference and training data [7]. In this paper, we introduce a new deep learning approach for HAR based on the notion of transformers and call it HART for Human Activity Recognition Transformer. HART is a lite-weight, sensor-wise transformer architecture specifically adapted for the IMUs-based Human Activity Recognition domain. Our experiments on representative datasets show that HART, compared to previous approaches, uses fewer FLOPS and parameters while outperforming current state-of-the-art results.

Precisely, this paper makes the following novel contributions:

- The HART and MobileHART architecture, a lighter and more robust transformer model based on ViT [8] and MobileViT [9], respectively, has been specifically adapted for the HAR domain.
- A systematic evaluation of different versions of HART, MobileHART, CNN, and CNN-LSTM on five publicly available datasets, not only in terms of performances (F-score) but also in terms of model size and computing cost.
- The actual performances of all the implemented models on a smartphone to report inference time and memory footprint.
- A quantitative evaluation of the robustness of the model to domain shifts such as unseen mobile positions and unseen device brand together with a qualitative analysis of the representation space of the model.
- Further experiments showing the impact of each new feature of HART (Multiheaded Self-attention & LiteConv) the impact of the capacity as well as the ability to handle several sensors.
- All code and datasets partitioning will be released for better reproducibility.

The paper is organized as follows. First, some background about Human Activity Recognition and Transformers is provided in Section 2. Then, our proposed models, HART and MobileHART, is detailed in Section 3. Section 4 details our environmental setup and learning configurations. Section 5 presents the evaluation results of the studied models on performances, efficiency, and robustness on five relevant public HAR datasets. Finally, the paper concludes based on our main findings and an outlook on future work.

2 Background & Related Works

2.1 Human Activity Recognition

Human Activity Recognition (HAR), on Inertial Measurement Units (IMU) based mobile devices, is the task of identifying daily human activities such as walking, running, and jumping from readings on time-series data. The domain generally makes use of a combination of accelerometers, a sensor that details proper acceleration, and gyroscopes, a device that senses angular velocity [10, 11]. HAR on mobile devices has essentially been used for healthcare monitoring and indoor positioning systems as an integration into pervasive environments [3, 12, 13].

Works in this domain necessitate solutions that achieve good performances and require the solution to be low cost regarding size and computation requirements that may run on low-powered devices. Recent studies in HAR [14, 5], for instance-based classification, have adopted lite-weight neural networks and have generally found success with lite-weight and shallow CNNs [15, 16] to achieve state-of-the-art results and resource requirements. Time-series data on IMU-based sensors are collected priory and then windowed to create frames of activity instances which are then fed into a neural network for the activity predictions and learning.

Despite recent advances and success in the Vision and Natural Language Processing domains with Transformer-based architectures [17, 8], only a few studies have adopted the architecture in the HAR domain for supervised learning tasks

[18, 19, 20, 21]. These studies have generally neglected the computation and memory cost of the proposed model. They do not consider the difference in sensor inputs (e.g., inputs can be from an accelerometer, gyroscope, and more) in the HAR domain. To our knowledge, only a recent study by [22] has presented an efficiency study on transformer-related architectures in the HAR domain.

2.2 Vision Transformer

Vision Transformer (ViT) [8], is the adapted work for the vision domain of the proposed Transformer-based architecture by Vaswani [17]. The original work by [17] proposes the use of Multi-Headed Self-Attention to dynamically enable the model to give more weight to certain segments of the inputs –which are referred to as patches in the ViT paper– over other segments during the inference. From the original Transformer architecture, ViT only uses the encoder part for image classification. ViT takes as input, an image (\mathbf{x}) with shape $H \times W \times C$ (Height, Width, Channel) which is first split into P patches, with fixed patch size $m \times m$, to produce $\mathbf{x}_p \in \mathbb{R}^{m^2 \cdot C}, p = 1, 2, \dots, P$. Each patch is then linearly projected in a dimensional latent space of size d and summed with $\mathbf{i}_p \in \mathbb{R}^d$ learnable position embeddings. The process can be expressed as below:

$$\mathbf{e}_0^p = \text{linearProj}(\mathbf{x}_p) + \mathbf{i}_p \quad \mathbf{e}_0^p \in \mathbb{R}^d, p = 1, 2, \dots, P$$

where \mathbf{e}_0^p is the projection of the patched image. The projected patches, together, can be expressed as $\mathbf{E}_l = \{\mathbf{e}_l^p \in \mathbb{R}^d \mid p \in \mathbb{N}, 1 \leq p \leq P\}$ where l is the current layer out of the total L encoder blocks. A learnable class token $\mathbf{CLS}_0 \in \mathbb{R}^d$ is then appended along with the patches at index 0, which results in a projection shape of $((P + 1), d)$ per inputted image. The resulting concatenation is then fed as the input to the first ViT encoder block, which is composed of Multiheaded Self-Attention (MSA), Feed Forward (FF), and Layer Normalization (LN) layers. There is a total of L encoder blocks, where each encoder block produces the next iteration of class token \mathbf{CLS}_l and embeddings \mathbf{E}_l . Put together, the processes here can be summarised as below:

$$[\mathbf{CLS}_l, \mathbf{E}_l] = \text{ViTEncoderBlock}_{l-1}([\mathbf{CLS}_{l-1}, \mathbf{E}_{l-1}]) \quad l = 1, 2, \dots, L$$

At the output of the last encoder block, only the class token \mathbf{CLS}_L is processed by a Feed-Forward Layer before the final output is mapped to the neural classification head to generate a predicted class probability distribution \mathbf{y} . The procedures here can be summarized as follow:

$$\mathbf{y} = \text{ClassHead}(\text{FF}(\mathbf{CLS}_L))$$

ViT and other models based on it have found much success in producing state-of-the-art results in image processing domains [23, 24] and have been the building block for many pre-trained models such as, to mention a few, DINO [25], MAE [26], and MOCOv3 [27]. However, much of the research effort has focused mainly on performance improvement, with only a relative handful of work also considering efficiency [28, 9, 29, 30]. Since MSA has a quadratic complexity with the input length $O((P + 1)^2 d)$, Transformer models such as ViT can be heavyweights. For this reason, widespread usage of classical transformers in mobile and other low-resourced devices has yet to be adopted.

2.3 MobileViT

Recently, a lightweight and general-purpose vision transformer called MobileViT has been presented [9]. Since transformer-based architectures focus on input-adaptive weighting and global processing, they lack coverage of the spatial inductive biases that CNN-based network learns. For this reason, MobileViT combines the two architectures and allows the model to encode both local and global information with fewer parameters. To do so, MobileViT integrates the relatively inexpensive inverted residual blocks from MobileNetV2 [31], composed of a series of stacked convolutional layers, with the power of a MobileViT block, an expanded version of the ViT encoder block.

The inverted residual blocks, which shall be referred to as the Mv2 (MobileNet Version 2) block for coherency purposes, are composed of point-wise ($PCov$) and depth-wise ($DCov$) convolutional layers [32]. The entire Mv2 block can be expressed as so:

$$\text{Mv2}_{\text{stride}=\{1|2\}}(\mathbf{x}) = \begin{cases} PCov(DCov_{\text{stride}=1}(PCov(\mathbf{x}))) + \mathbf{x} \\ PCov(DCov_{\text{stride}=2}(PCov(\mathbf{x}))) \end{cases}$$

Given input embedding $\mathbf{x} \in \mathbb{R}^{H,W,C}$, it is first passed through a point-wise convolutional layer to project the input to the latent dimension. The resulting outputs are then passed through a depth-wise convolutional layer, either with a stride of 1 or 2 (for downsampling). Finally, the outputs are then given to another point-wise convolutional layer which is then added –only when there is no downsampling– with the original \mathbf{x} input through a residual connection. All convolutional operations are followed by batch normalization and a non-linear activation.

MobileViT block's is composed of $SConv()$ standard convolutional, $PConv()$ point-wise convolutional and the encoder block of ViT. The entire process of the block can be formulated as:

$$AOut(\mathbf{x}) = ViTEncoderBlocks_L(PConv_1(SConv_1(\mathbf{x})))$$

$$MobileViTBlock(\mathbf{x}) = SConv_2(Concat(PConv_2(AOut(\mathbf{x})), \mathbf{x}))$$

$SConv_1(x)$ projects and splits inputs x into P patches and encodes local spatial information. The second $SConv_2()$ is used as a method of fusion between the concatenated inputs and attention outputs ($Concat(PConv_2(AOut(\mathbf{x})), \mathbf{x})$). The point-wise convolutions ($PConv_1$ & $PConv_2$) projects the embedding to a higher dimensional space. Note here that positional encoding is no longer used in MobileViT as the integration of convolutional networks into the architecture to learn spatial inductive biases.

MobileViT has shown improvement over related architectures [32, 33] as well as competitive results against large models [34]. MobileViT is faster than large CNNs [34] but is slower than lightweight CNNs [32] in terms of both inference and training time. This property is mainly due to MSA layers of transformers that lack dedicated device-level operations support as compared to CNNs [9].

2.4 LightConv

As previously stated, the complexity of MSA is quadratic with the input size and is proportional to the embedding size d . In order to diminish the computing burden, Wu *et al.* [35] has split the embedding dimension d by half, where one-half feeds a LightConv block [36] while the remaining half feeds an MSA layer. This approach effectively reduces the number of operations performed by the MSA layer. It allows the MSA to focus on capturing the global relationship between inputs instead of local relationships between neighboring segments/patches. Compared to self-attention, LightConv has a fixed context window, and it determines the importance of context elements with a set of weights that do not change over time steps. Hence, the combination between the MSA and LightConv layers allows the model to be faster and requires significantly fewer parameters ($H * k$) with H Attention Head and K Kernel Size. The LightConv block, as presented in the original work [36], is computed as follow:

$$LightConv(\mathbf{x}) = SoftMaxDCConv(\mathbf{x})$$

where $SoftMaxDCConv()$ is a depth-wise convolutional layer that has been normalized over the kernel dimension with a softmax function.

3 Human Activity Recognition Transformer

This section introduces Human Activity Recognition Transformer (HART), a lightweight transformer architecture specifically designed for embedded IMU sensing devices. Figure 1 provides an overview of the HART architecture adapted from ViT, where much of the changes from ViT are at the MSA layer within the encoder and linear projections layer. In order to better suit such architecture for HAR, it necessitates the model to be lightweight (few parameters & low complexity) so that both goals of real-time inference capability and low energy consumption can be reached. Furthermore, the model should be adapted to data that can potentially be from multiple channels and sensors (e.g., accelerometers, gyroscopes, magnetometers, and others).

3.1 Overall architecture

The input to HART (cf. Fig. 1) is a window of data $\mathbf{x} \in \mathbb{R}^{W,3*S}$ of W window time-length, composed of data provided from S sensors, each having three channels (X, Y, Z axis). In practice, the continuous input data is segmented by a window of size W samples without overlap. For the remainder of the paper, we use a setting where $S = 2$ since most datasets contain only accelerometer and gyroscope data. However, HART can accommodate more sensors, which is later shown in section 6.3.

At the beginning of the HART process, \mathbf{x} is framed and linearly projected, in a sensor-wise manner, by specific convolutional layers for each sensor data. Here, framing is equivalent to patching for the vision domain, where a window of IMU data is partitioned into multiple frames of smaller lengths. With the sensor-wise convolutions, in the case where we have only have accelerometer and gyroscope as inputs, there would be an accelerometer-oriented convolutional layer that processes $\mathbf{x}_{acc} \in \mathbb{R}^{W,3}$ and a gyroscope-oriented convolutional layer that process $\mathbf{x}_{gyro} \in \mathbb{R}^{W,3}$. Given

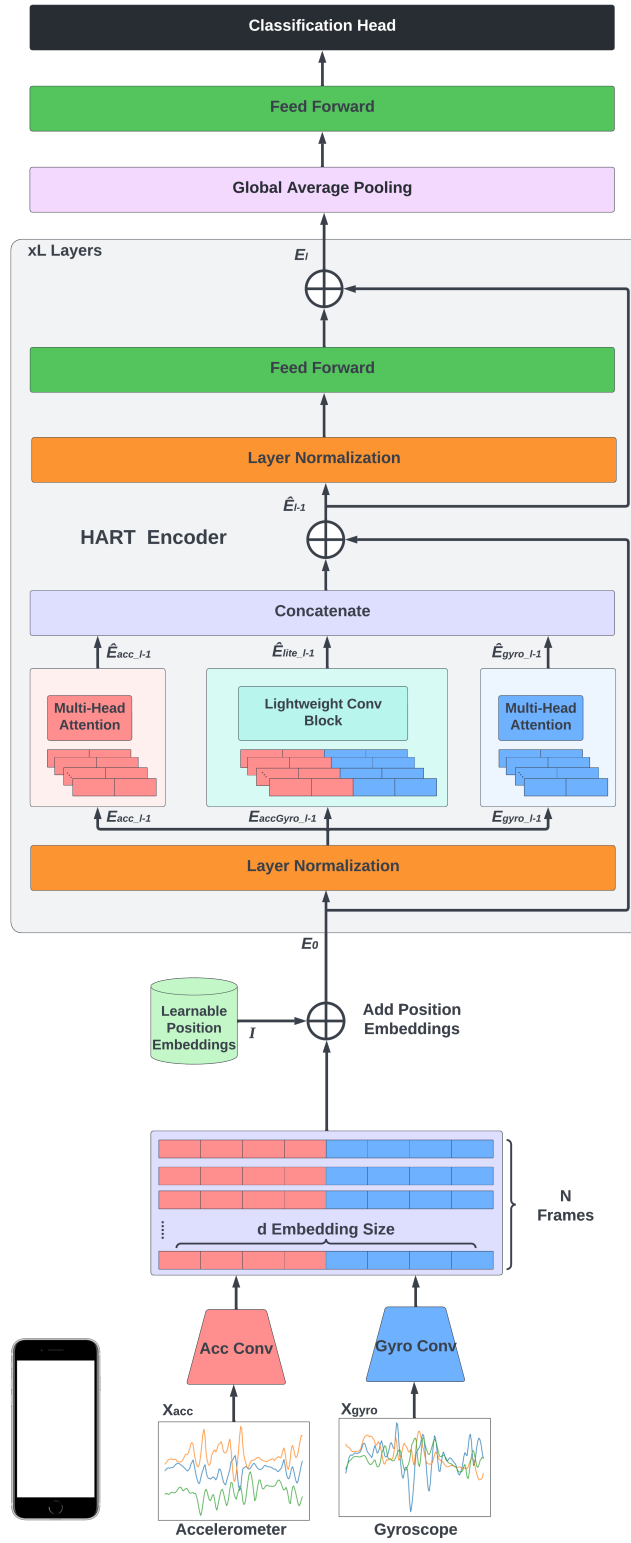


Figure 1: Overview of HART

hyper-parameter embedding dimension d , each sensor-wise convolutional layers have d/S amount of filters with kernel size of $K \times 1$. Altogether, each sensor-wise convolution layer, with a stride equal to the kernel size, generates non-overlapping frames of size d/S . The projection of the accelerometer and gyroscope input data generates N embeddings composed of $\hat{\mathbf{x}}_{acc} \in \mathbb{R}^{N, d/S}$ and $\hat{\mathbf{x}}_{gyro} \in \mathbb{R}^{N, d/S}$. The two outputs of the convolutional layers are concatenated together to form the projected embedding vectors. This embedding vectors are then added to learnable position embeddings $\mathbf{I} \in \mathbb{R}^{N, d}$ to finally have $\mathbf{E}_0 \in \mathbb{R}^{N, d}$. Note here that for HART, we do not append a learnable class embedding to $\hat{\mathbf{x}}$ and instead favor the use of Global Average Pooling (GAP), which reduces computation cost and parameters with no loss in performances [29]. The operations all together can be written as below:

$$\mathbf{E}_0 = \text{concat}(\text{Conv}_{acc}(\mathbf{x}_{acc}), \text{Conv}_{gyro}(\mathbf{x}_{gyro})) + \mathbf{I}$$

\mathbf{E}_0 will be used as the first HART encoder input, which is then processed with layer normalization to standardize the embeddings across different sensors. Since the normalized embeddings were initially concatenations from two different sensors, we can separate back the accelerometer and gyroscope embedding vectors. HART partitions and uses the different embeddings as follows: half of the accelerometer embeddings $\mathbf{E}_{acc} \in \mathbb{R}^{N, d/4}$ are processed by an accelerometer-wise Multiheaded Self-Attention ($MSA_{acc, l}$); half of the gyroscope embeddings $\mathbf{E}_{gyro} \in \mathbb{R}^{N, d/4}$ are processed by a gyroscope-wise Multiheaded Self-Attention ($MSA_{gyro, l}$); while the remaining half of both sensors embedding $\mathbf{E}_{accGyro} \in \mathbb{R}^{N, d/2}$ are left concatenated and passed to a *LightConvBlock* to capture the local relationship and to allow sensor-wise MSA to focus more on global relationship. In addition, as we combine accelerometer and gyroscope embeddings with the *LightConvBlock*, we get an early fusion of the sensor’s knowledge. The outline of the process is presented below:

$$\mathbf{E}_{acc, l-1}, \mathbf{E}_{gyro, l-1}, \mathbf{E}_{accGyro, l-1} = LN_{l-1}(\mathbf{E}_{l-1}) \quad l = 1, 2, \dots, L$$

$$\hat{\mathbf{E}}_{acc, l-1} = MSA_{acc, l}(\mathbf{E}_{acc, l-1})$$

$$\hat{\mathbf{E}}_{gyro, l-1} = MSA_{gyro, l}(\mathbf{E}_{gyro, l-1})$$

$$\hat{\mathbf{E}}_{lite, l-1} = \text{LightConvBlock}_l(\mathbf{E}_{accGyro, l-1})$$

Where, $\hat{\mathbf{E}}_{acc, l}$, $\hat{\mathbf{E}}_{gyro, l}$ and $\hat{\mathbf{E}}_{lite, l}$ are computed in parallel when the host device supports parallel operations. Such architecture allows HART to take advantage of any available on-device GPU to reduce the computation load and inference time. In addition, by adopting the sensor-wise MSA, the model can be separately attentive to different sensor inputs rather than a single attention map over all sensors, as illustrated in Figure 2. This trait allows specialized attention over individual sensors instead of compromised attention between the two.

The attention mechanism of transformer-based architectures has a complexity that depends on the sequence length, and the projection size d [17]. Thus, splitting the input embedding size to only $1/4$ of d for each sensor-wise MSA can effectively diminish computation needs (without decreasing performances, as experiments will reveal). The original complexity of $O(N^2d)$ of MSA layers would be reduced to $O(2(N^2d/4))$.

Afterwards, we concatenate $\hat{\mathbf{E}}_{acc, l-1}$, $\hat{\mathbf{E}}_{gyro, l-1}$ and $\hat{\mathbf{E}}_{lite, l-1}$ together, with their original position kept in place, to create $\hat{\mathbf{E}}_{l-1}$. The subsequent processes then follows the structure of a classical ViT encoder [8] and all together can be formulated as below:

$$\hat{\mathbf{E}}_{l-1} = \text{concat}(\hat{\mathbf{E}}_{acc, l-1}, \hat{\mathbf{E}}_{gyro, l-1}, \hat{\mathbf{E}}_{lite, l-1}) + \mathbf{E}_{l-1}$$

$$\mathbf{E}_l = \text{HARTEncoderBlock}_l = FF_{l-1}(LN(\hat{\mathbf{E}}_{l-1})) + \hat{\mathbf{E}}_{l-1}$$

Here, the FF layer will fuse the embeddings from the two sensor-wise MSA and LightConv blocks together. However, the residual connection at \mathbf{E}_l still influences the outputs values by their sensor-wise position within the vector. Such property fades as more blocks process the embeddings in the upper blocks.

Lastly, in our study, the outputs of the last HART encoder block are combined through a GAP layer, where the outputs are passed to a feed-forward layer and then finally given to the classification heads.

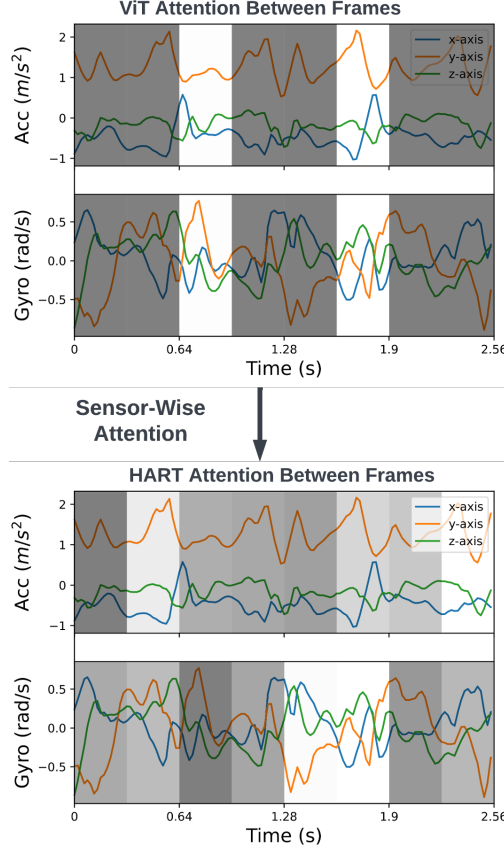


Figure 2: Comparison of ViT’s attention map and HART’s attention map for a window of the upstairs activity.

3.2 Shared Multiheaded Self-Attention

To further reduce the number of parameters, the computation time, and memory usage of the MSA, we propose to use only one MSA in HART to operate individually and in parallel on different sensor inputs. We call this configuration $\text{HART}_{\text{OneMSA}}$, where a single MSA with projection size $d/4$ operates indistinctly on accelerometer input embeddings $\mathbf{E}_{\text{acc}_{l-1}} \in \mathbb{R}^{N, d/4}$ and gyroscope input embeddings $\mathbf{E}_{\text{gyro}_{l-1}} \in \mathbb{R}^{N, d/4}$. Hence, the computation of $\hat{\mathbf{E}}_{\text{acc}_{l-1}}$ and $\hat{\mathbf{E}}_{\text{gyro}_{l-1}}$ from the previous section becomes:

$$\hat{\mathbf{E}}_{\text{acc}_{l-1}} = \text{MSA}_{\text{one}_l}(\mathbf{E}_{\text{acc}_{l-1}})$$

$$\hat{\mathbf{E}}_{\text{gyro}_{l-1}} = \text{MSA}_{\text{one}_l}(\mathbf{E}_{\text{gyro}_{l-1}})$$

where the two $\text{MSA}_{\text{one}_l}$ above are the same MSA that individually project two sensor-wise attention maps for the accelerometer and gyroscope embeddings. This design is possible and beneficial due to the layer-normalization done priorly that effectively reduces variances between the sensors and allows a single MSA weight to be used for both sensors.

3.3 MobileHART

As previously mentioned, MobileViT integrates ViT encoder and CNNs to allow transformer-based architectures to learn spatial inductive bias [9]. Here, we raise that for instance-based human activity recognition, where time-series data are framed, we can also learn temporal inductive bias by adopting the same process as MobileViT [37]. Similarly, we would have every time-step in the frame contain encoded information of its neighbors.

Therefore, we adapted MobileViT to suit the HAR domain better and refer to the architecture as MobileHART. As illustrated in Figure 3, we make use of sensor-wise convolutional layers and sensor-wise inverted residual blocks

(AccMV2, GyroMV2) to process sensor inputs separately. The outputs of two sensors’ convolutional processes are concatenated to form the inputs to the MobileHART block, which is a MobileViT block that now uses sensor-wise convolutions ($PConv_{SW}$ & $SConv_{SW}$) and a HART encoder. We note that the sensor-wise operation is performed only up to the input of the MobileHART block, where afterward, the features from different sensors are fused. The entire process described here replaces the $AOut()$ of the $MobileViTBlock()$ mentioned previously in section 2.3 to the below:

$$AOut(x) = HARTEncoderBlocks_L(PConv_{SW}(SConv_{SW}(x)))$$

where $x \in \mathbb{R}^{N,d}$ is a feature embedding that has been processed by multiple layers of accelerometer and gyroscopes MV2 blocks. Afterward, the remaining operations follow the original MobileViT architecture process that has been adapted to fit one-dimensional time-series data, where we use 1D convolutions over the 2D variant.

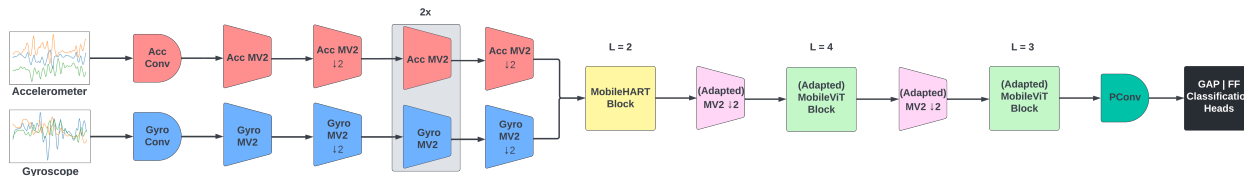


Figure 3: Overview of MobileHART

4 Experiments & Configuration

This section details the datasets and configurations used in the experiments done during this study. In order to evaluate HART in multiple settings and scenarios, we have selected a total of five different datasets, each presenting different traits and environments. We detail as much as possible the dataset partitioning we use and training configurations of our study to allow reproducible results across all our studies.

4.1 Datasets

The **UCI HAR** dataset [38] was collected with a Samsung Galaxy S II, which had a sampling rate of 50 Hz, and was positioned on the subject’s waist. The dataset accounts for about 3.6 hours of recorded activities. The experiments were conducted on 30 participants with an age range of 19-48 years old. The UCI dataset has six activities (Walking, Upstairs, Downstairs, Sitting, Standing, and Lying) and was collected in a closed & controlled indoor lab environment using artificial situations. Despite the UCI dataset being very homogeneous and not ecological, it comes with a pre-partitioned Train and Test set that favors reproducibility and is very popular in the HAR research community since it has been used to compare the state-of-the-art methods. Hence, even if the dataset is too homogeneous and small, we include it as a benchmark dataset that allows performance comparison across different studies.

The **MotionSense** dataset [39] had 24 subjects, with a variety of ranges regarding gender, age, weight, height, performing 15 long trials with a duration of 2-3 minutes and 6 short trails that last from 30 seconds to 1 minute. There are six activities: Downstairs, Upstairs, Sitting, Standing, Walking, and Jogging/Running. The test was conducted in the same environment for all subjects using an Apple iPhone 6s, with a sampling rate of 50 Hz, that was kept in the subject’s front pocket. Collected data were from an on-device accelerometer, attitude, and gyroscope sensors. The Motionsense dataset was collected to identify attribute-specific patterns that can be used to infer the gender or personality from the subject’s sensor data. Motionsense is also a dataset that has often been used in the community despite its small size and the fact that it comes without official train/test partitions [40, 11].

The **Heterogeneity Human Activity Recognition (HHAR)** dataset [41] accounts for 4.5 hours of recorded activities. Each of the 9 participants carried 8 Android smartphones (two LG-Nexus 4, two Samsung Galaxy S3, two Samsung Galaxy S3 Mini, and two Samsung Galaxy S+) within a compact pouch and four Android smartwatches (two LG watches and two Samsung Galaxy Gears) on the arm, were asked to perform five minutes of six activities (Biking, Sitting, Standing, Walking, Upstairs and Downstairs). All 12 devices recorded the activities using the on-device accelerometer and gyroscope measurements to their respective maximum sampling rate (between 50 Hz and 200 Hz). Additionally, the authors of the dataset highlighted that the devices have gone through previous daily-life usage and hints of real-life induced usage errors on the recording device. Though not very large, the HHAR dataset is interesting to us since it depicts a very systematically heterogeneous learning environment due to the array of different devices used in the data collection. As for other datasets, it comes without official train/test partitions.

The **RealWorld** dataset [42], which contains 18 hours of recorded data, including accelerometer and gyroscope readings. The data were collected in 2016 from 15 subjects in 7 different devices and body positions, using Samsung Galaxy S4 and LG G Watch R with a sampling rate of 50 Hz. The recording was performed outdoors, where the subjects were told to perform specific activities without any restraints. Eight activities have been labeled in the data: Downstairs, Upstairs, Lying, Sitting, Standing, Walking, Jumping, and Running. We believe the RealWorld dataset represents HAR data well in the wild and exhibits a realistic high-class imbalance (for instance, the ‘standing’ activity represents 14% of the data while the ‘jumping’ one is limited to 2%). Furthermore, it is one of the largest available datasets of this kind. Finally, since the dataset was recorded from the 7 different devices and body positions (chest, forearm, head, shin, thigh, upper arm, and waist), it presents a very statistically heterogeneous learning environment. Unfortunately, no official train/test partitions are provided.

The **Sussex-Huawei Locomotion (SHL)** Preview dataset [43] is composed of 59 hours of annotated recordings acquired in 2017. It was recorded by 3 different users throughout their daily lives, each over a period of 3 days, with 4 different devices and body positions. We only considered the accelerometer and gyroscope data for our experiment. The data were collected using only Huawei Mate 9 smartphones with a sampling rate of 100 Hz. Each user was recorded in 3 distinct time sessions, and each focused on different locomotion styles and activities. The SHL dataset has 8 labels: Still, Walking, Run, Bike, Car, Bus, Train, and Subway. The dataset is very large compared to previous datasets and presents challenging classification tasks on locomotion-based activities. We note that while we are aware of the Sussex-Huawei Locomotion Challenge 2020 dataset’s prepartition, their relatively large train data were only comprised of 1 user’s activities. As our study emphasizes a heterogeneous learning environment, where the learning data holds many characteristics, we instead favor characteristics and utilize the SHL preview configuration.

Table 1: Datasets properties

Dataset	Data Samples	Activities
UCI	10,299	6 (ST,SD,W,U,D,L)
MotionSense	17,231	6 (ST,SD,W,U,D,R)
HHAR	85,567	6 (ST,SD,W,U,D,BK)
RealWorld	356,427	8 (ST,SD,W,U,D,J,L,R)
SHL Preview	640,144	8 (ST,W,R,BK,C,BS,T,SW)
Combined	1,109,668	13 Unique Activities

All together, Table 1 shows the number of data samples per dataset and the different activities. In total, The datasets contain 13 unique activities: Walk (W), Upstairs (U), Downstairs (D), Sit (ST), Stand (SD), Lay (L), Jump (J), Run (R), Bike (BK), Car (C), Bus (BS), Train (T), Subway (SW). In terms of class distribution, “Jump” is the minority class, while there are many samples for the “Stand” and “Walk” classes.

As the datasets were recorded with different sampling rates, we downsampled all datasets to 50 Hz after having applied an Anti-Alias filter. Such sampling frequency is in line with a survey regarding HAR on smartphones [44] that have shown that the optimal sampling frequency is between 20 Hz and 50Hz and that accelerometers and gyroscopes are the most adequate sensors for classification. Using sampling rates beyond 50Hz would incur more extensive computation, and memory costs with only a marginal gain in performance [44].

4.2 Partitioning and Pre-processing

Out of the five presented datasets, only the UCI dataset came pre-partitioned with a train and test set. Thus, we used this dataset for comparison using the same test partition. Regarding pre-processing, after downsampling (when applicable), we only used raw signals that we normalized using channel-wise z-normalization. This standard is different from other state-of-the-art studies on the UCI dataset [45, 46, 22] where they make use of the already hand-crafted data offered by the dataset or apply their pre-processing techniques on the raw form of the dataset. In this work, the representation (i.e., features) are learned; they are not hand-crafted.

We applied the same pre-processing to the remaining four datasets: MotionSense, HHAR, RealWorld, and SHL. We partitioned each dataset following a 70% train-set, 10% development-set, and a 20% test-set partition according to each participant’s recorded activities. We used a window-frame size of 128 (2.56s) with an overlap of 50% over the 6 channels from the accelerometer and gyroscope sensor.

All experiments were performed using the same train, validation, and test sets for each dataset. We have made our code and the dataset partition publicly available to make our work easily reproducible ¹.

¹<https://github.com/getalp/Lightweight-Transformer-Models-For-HAR-on-Mobile-Devices>

4.3 Learning Environment & Hyper-parameters

To the best of our abilities, we attempt to replicate the training hyper-parameters from their original work and make the models comparable across the different architectures.

All learning experiments were conducted on a high-performance computing cluster utilizing Intel Cascade Lake 6248 processors with 192GB of memory and Nvidia Tesla V100 SXM2 16GB GPUs. We use TensorFlow for the development of all models in this study [47].

We perform 200 epochs of class-weighted training to deal with high-class imbalance for all our experiment settings while using a mini-batch size of 32. We then use a label smoothing rate of 0.1 to prevent over-fitting. Across all learning instances, we employ Adam [48] as the learning optimizer with a learning rate of 0.0005. We note here that it is possible to further improve the results across all models when we instead employ AdamW [49], where we precisely tune the weight decay for each architecture. Although, this was beyond the scope of the study, where the objective was to replicate a comparable environment of shared training configurations to evaluate different architectures with similar settings.

Specifically for transformer-based models hyper-parameters, after several experiments and based on other studies on low resourced data [50], we settle on a dropout rate of 0.3 after most feed-forward layers. We note that our dropout rate is much higher than the usual choices with respect to other works on transformer-based models; usually, a rate of 0.1 - 0.2 [8, 35, 25]. This choice is because, as opposed to the vision or language domain, the size of the datasets in the HAR domain is significantly smaller, which makes the models more prone to overfitting. As an extension to counter overfitting, we also apply DropPath with regards to the stochastic depth rule before every residual connection [51, 52]. Extensively, on model configuration choices, we found that swish activation [53], in-line with other studies [9], gave better results than the classical GELU activation [54] used in transformer-based models.

For ViT and HART, we adapt the "ViT Tiny" configuration [25] with an embedding size of $d = 192$ and attention head counts of $H = 3$. Six layers ($L = 6$) out of the 12 layers of the original study were used [8]. Input window data of $W = 128$ samples are split into frames of 16 samples (0.32s) with a stride of 16 (No overlap) for the segmenting.

We note here that experiments done with overlap (a time-step below 16) showed only marginal improvement in performances but incurred significantly higher costs as the model resulted in more data to process. Thus with the following setup, we obtain 8 frames for self-attention.

For our configuration with MobileViT and MobileHART, two network configurations were implemented: extra small (XS) and extra extra small (XXS), as done by the original study [9]. We note that the difference between configurations XS and XXS are characterized by the number of filters, their expansion factors that dictate the filter's growth after each MV2 layer, and the embedding size of the MobileViT/MobileHART blocks. The number of layers and attention heads is the same between the two configurations.

5 Studies & Results

5.1 Evaluations & Comparisons

We first present our results on the pre-partitioned UCI dataset, here shown in Table 2, then afterward on the remaining four datasets, as shown in Table 3. We compare HART against ViT with the same hyper-parameters, a two-layered CNN [15] that has shown good performance on both small and large datasets [55] and a lightweight CNN-LSTM [56]. Finally, we evaluate the same model's efficiency on a smartphone.

Table 2 shows the F-score, parameters, and FLOPS for all architectures. Here, we can observe that all versions of HART outperform their respective counterparts (ViT, MobileViT). The HART architecture led to an increased F-scores between 0.1% - 0.7%, a 5% minimum decrease in parameters, and at least a 9% decrease in FLOPS. HARTs' main contribution is its reduction and sensor-wise MSA, and additional gains are further studied in section 6.2 where the layers, embedding size, and amount of heads are increased. MobileHART (XXS) obtained the overall best performance with an F-score of 97.67%, 3% higher than the best non-transformer-based approaches (CNN had an F-score of 94.53% and the CNN-LSTM performed the worst with 92.79%). ViT under-performs in this environment with an F-score of 93.66%, which is likely due to the low amount of training data of UCI. We can also note that MobileViT/MobileHART does not improve performance with increased dimension size on the UCI dataset. MobileHART (XS), with an F-score of 97.20%, performed slightly worst than MobileHART (XXS).

The lite CNN-LSTM, naturally, has the smallest parameters and FLOPS amongst all the studied model. Amongst transformer based-architectures, it is MobileHART (XXS) that has the least amount parameters (1,275,702) and FLOPs (8,213,276). MobileViT (XXS) with parameter count of 1,352,054 and a FLOPS of 8,995,612, has about 5% more

Table 2: Results on the pre-partitioned UCI dataset

Architecture	F-Score (\uparrow)	Parameters (\downarrow)	FLOPS (\downarrow)
CNN	94.53	6,448,714	17,725,476
CNN-LSTM	92.79	559,558	1,350,180
ViT	93.66	3,783,238	17,069,949
HART	94.49	1,445,918	15,212,636
HART _{OneMSA}	94.37	1,277,150	15,176,924
MobileViT (XS)	96.89	2,734,622	22,983,180
MobileHART (XS)	97.20	2,542,942	19,809,292
MobileViT (XXS)	96.55	1,352,054	8,995,612
MobileHART (XXS)	97.67	1,275,702	8,213,276

Table 3: The F-Scores on five datasets

Architecture	UCI	MotionSense	HHAR	RealWorld	SHL	Combined
CNN [15]	94.53	96.91	96.99	91.71	87.08	86.87
CNN-LSTM [56]	92.79	97.80	96.97	92.33	88.92	88.03
ViT [8]	93.66	98.09	97.39	94.57	93.11	93.52
HART [Ours]	94.49	98.13	98.31	95.49	94.39	94.59
HART _{OneMSA} [Ours]	94.37	98.29	98.28	95.74	94.88	94.07
MobileViT (XS) [9]	96.89	98.19	98.65	95.07	94.14	93.19
MobileHART (XS) [Ours]	97.20	98.49	98.72	95.81	94.86	94.24
MobileViT (XXS) [9]	96.55	98.42	98.30	93.72	91.46	91.07
MobileHART (XXS) [Ours]	97.67	98.32	98.19	94.32	92.60	91.91

parameter and around 8% less FLOPs than MobileHART (XXS). When we compare ViT to HART, we see observe more than 61% decrease in parameters (3,783,238 vs 1,445,918) and about a 10% decrease in FLOPS (17,069,949 vs 15,212,636). HART_{OneMSA} was able broaden the gap with approximately 66% reduction in parameter count (3,783,238 vs 1,277,150) and 11% decrease regarding FLOPS (17,069,949 vs 15,176,924).

Table 3 presents the F-score across different model architectures on the 4 datasets, RealWorld, HHAR, MotionSense and SHL. In addition, we combine all the 5 datasets to generate the largest dataset with high diversity for our evaluation. The combination results in 13 unique activities to predict data with a high-class imbalance from many different devices and positions. As specified in Section 4.3, we used class-weighted training to deal with the high-class imbalance.

On all datasets, we can see that all attention-based models outperformed standard approaches such as CNN and CNN-LSTM. It appears that the larger the dataset, the larger the margin of the F-score between the transformation-based approach and the standard approach. MobileHART (XS) obtained the best performance on the multi-positioned RealWorld dataset with an F-score of 95.81%, around 0.7% higher than MobileViT (XS). In addition, MobileHART (XS) outperforms other architectures/configurations on the multi-device HHAR and apple-device-based MotionSense with an F-score of 98.72% and 98.49%, respectively. On the large SHL Dataset, HART_{OneMSA} obtained the best performance with an F-score of 94.88% similar to MobileHART (XS), only short of 0.02%. Finally, on the combination of all 5 datasets, HART obtained the best performance with an F-score of 94.59%, around 9% higher than the CNN-based approach.

Overall, we are able to see different behavior according to the size and the degree of heterogeneity of the datasets. On the UCI dataset, the CNN was very competitive with performances of the ViT model we adapted to the HAR task. But, on larger datasets, the CNN architecture underperforms. The CNN-LSTM, the most lightweight model in our evaluation, performed much better in terms of cost and performance than the CNN. However, the performance degrades significantly with large datasets such as the SHL and the combined datasets. On the contrary, the transformer-based model on these large benchmarks, where ViT, HART, and MobileHART outperform other approaches with more data. While the adapted ViT under-performed on UCI, it outperformed the CNN and CNN-LSTM models on all other benchmarks. HART exhibited very similar performance across the different datasets but could consistently outperform the ViT model in every case. HART_{OneMSA}, which further reduced parameters count over baseline HART, surprisingly presented outstanding performances (Beating HART in half of the datasets) and showed that a single multiheaded

Table 4: On-Device inference time and memory footprint over 1000 inferences

Architecture	Average Inference Time (μ s)	Memory (MB)	Model Size (MB)
CNN [15]	2143 \pm 452	51.05	25.80
CNN-LSTM [56]	1496 \pm 271	6.45	2.25
ViT [8]	8213 \pm 1518	32.07	15.22
HART [Ours]	5376 \pm 1104	12.74	5.91
HART _{OneMSA} [Ours]	4890 \pm 760	8.89	5.21
MobileViT (XS) [9]	11,341 \pm 6,124	23.14	11.07
MobileHART (XS) [Ours]	13,488 \pm 1,466	20.77	10.35
MobileViT (XXS) [9]	5,142 \pm 958	15.86	5.57
MobileHART (XXS) [Ours]	6,398 \pm 1,014	12.86	5.30

self-attention head could be enough to model inputs from multiple sensors individually. MobileViT (XS-XXS) and MobileHART (XS-XXS) were very competitive on the different datasets. All MobileHART architectures improved over their MobileViT counterparts. MobileHART, with size XXS obtaining the best results for the UCI dataset, showed that increasing the size of the dimensions for small datasets is not always beneficial (The more extensive XS configuration obtained a lower F-score). However, for the larger datasets, we see that MobileHART (XS) is the most performing model overall. It was the best for RealWorld, HHAR, and MotionSense and second-best in SHL and combined. We can observe hints of embedding size bottle-necks for MobileViT and MobileHART on the large SHL and combined datasets, as the size XS or XXS is insufficient to capture and process much different knowledge from large-sized datasets. The findings are in line with other studies, where transformer-based models require a more considerable amount of data to converge but can be more resilient on more tasks [57].

Our findings here show that despite a lower amount of parameters and fewer FLOPS, HART and MobileHART make it possible to combine lightweight models and performance beyond the current state-of-the-art. However, is this lighter model meet the efficiency requirements for low resource targets such as mobile phones? The following section answers this question.

5.2 On-Device Performances

We ported all models in our experiments, using TensorFlow lite, to a 2017 Google Pixel 2 with a Qualcomm MSM8998 Snapdragon 835 chipset (Octa-core CPU with 4x2.35 GHz Kryo & 4x1.9 GHz Kryo) and 4GB of RAM. Afterward, we use TensorFlow’s benchmark tools to measure the average inference time along with its standard deviation, the memory footprint, and the model size for over 1000 inferences using 4 threads with the different architectures². For technical reasons, all models were inferred using the on-device CPU.

The result of the experiments is presented in Table 4. The inference time of the models is between 1 to 13 ms for input data with a time length of 2.56 seconds. The transformer-based model with the longest inference time in our study, MobileHART (XS), can classify more than 76 samples per second, which is well above the real-time criteria of 28 samples per second set by another study [15]. This performance shows that all the models studied in this paper can achieve real-time activity classification.

We first see that the non-transformer-based approaches are much faster in inference speed, CNN with an inference time of 2143 μ s and CNN-LSTM coming the fastest with 1496 μ s. MobileViT (XS) and MobileHART (XS) have the longest inference time with, respectively, 11,341 μ s and 13,488 μ s. We stress that implementations of HART are developed to take advantage of parallel computations. If the workload is done sequentially or with little parallelization with a few threads, we may see additional inferences duration increase as observed between MobileViT and MobileHART. In addition, we mention here that for MobileViT and MobileHART, while they indeed have a lower amount of process and parameters, they require a larger inference time due to their relatively high number of stacked layers. Another aspect of HART is that when the dimension gets larger, HART, contrary to ViT, reduces the dimensions of MSA layers, effectively reducing complexity. This change led to a speed-up in inference time over ViT (8213 μ s) against HART (5376 μ s). Finally, HART_{OneMSA}, with 4890 μ s, has the best inference time compared to all other transformer-based models.

²Tensorflow-Benchmark tools - <https://www.tensorflow.org/lite/performance/measurement>

In terms of memory and model size during inference, we can establish a close relationship between the number of parameters. With roughly 6 million parameters, the CNN model takes up an overall 51.05 MB of ram for inference and 25.80 MB in storage space, the highest in footprints against other architectures. The CNN-LSTM, with about 559 thousand parameters, has the lowest memory and storage footprint of 6.45 MB and 2.25 MB, respectively. Comparing ViT and HART, it is striking to see far fewer costs in memory and storage requirements. HART requires around 60% less memory (32.07 MB vs. 12.74 MB) and about 61% less storage (15.22 MB vs. 5.91 MB). HART_{OneMSA} again has the best memory/storage footprint of the transformer architecture with a memory need of 8.89 MB and a storage requirement of 5.21 MB. For the MobileViT and MobileHART architectures with XS size, we see that the memory and storage cost is lower than ViT, whereas it was higher in terms of inference time. MobileViT had a memory and storage footprint of 23.14 MB and 11.07 MB, respectively. While MobileHART was able to decrease the cost by a small margin with a memory and storage footprint of 20.77 MB and 10.35 MB, respectively. Finally, MobileViT and MobileHART of size XXS have an excellent middle ground between the relatively expensive sized XS counter-part and the lighter baseline ViT and HART. MobileViT took up 15.86 MB and 5.57 MB, respectively, for memory and storage. MobileHART showed 12.86 MB and 5.30 MB, respectively, for memory and storage. The results here provide insights into actual performances on a real mobile phone, contrary to other works that simulate the process in the HAR domain. Our findings show that inference time is far below the data input duration. While the biggest memory footprint in our study is 50 MB, out of the available 4GB, much application runs in parallel on mobile devices, and as such, the model must be as small as possible.

5.3 Representation & Task Variances

The previous sections show that the lightweight Transformer model, though more demanding in computing than standard CNN-LSTM models, outperforms the latter by a significant margin. In this section, we want to understand better how these models get better performances. To do so, we conducted two studies to shed light on two aspects: the quality of the learned representations and the robustness to changes beyond learned data (i.e., domain shift).

In this section, we selected only the models with the best F-score of the three different kinds of architecture: CNN, HART, and MobileHART(XS). The representations were qualitatively assessed based on 1) How well different classes are separated from each other and 2) How closely intertwined the embeddings of the same class but of different origins are (e.g., the different positions of the mobile sensing devices during data collection, different device system, and others). We look into the representations of different models on the 7 body positions of the RealWorld (RW) dataset to assess the model’s robustness to *statistical heterogeneity*, which in HAR is often referred to as the different placement, orientation, or looseness of the sensing devices. Furthermore, we use the data of 6 different brands of devices provided by the HHAR dataset to observe the models versatility against *system heterogeneity*, which in our case refers to the model’s ability to perform on a different device from diverse manufacturers where their sensors may have different biases and margin of errors [41].

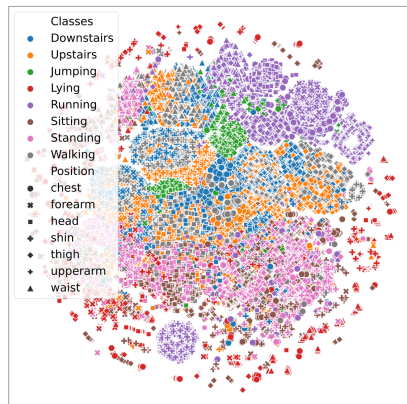


Figure 4: CNN RW

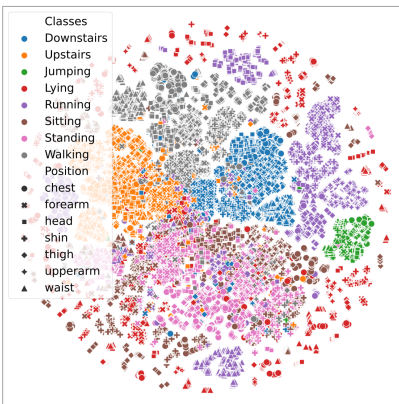


Figure 5: HART RW

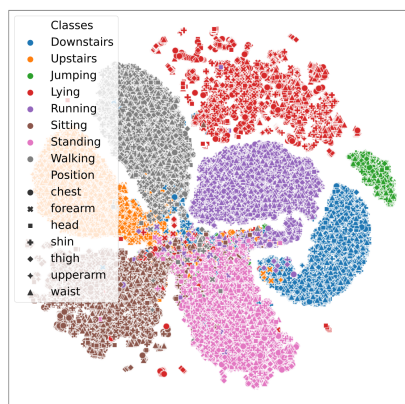


Figure 6: MobileHART (XS) RW

Figures 4 and 7 show the representations –using the dimensions reduced with T-SNE [58]– of the CNNs that were trained on the RW and HHAR datasets on their respective test-set. Here we observe that there is indeed a degree of separation of classes. On the RW dataset, many classes are too intertwined, such as the representations between ‘Downstairs’ and ‘Upstairs’ activities and, in another case, the ‘Standing’ and ‘Sitting’ class. In addition, we see a separation of the positions, exemplified by the Running class, where the ‘Upperarm’ position forms a separate cluster far away from all other positions. Moreover, the ‘Lying’ activity instances were not clustered but distributed

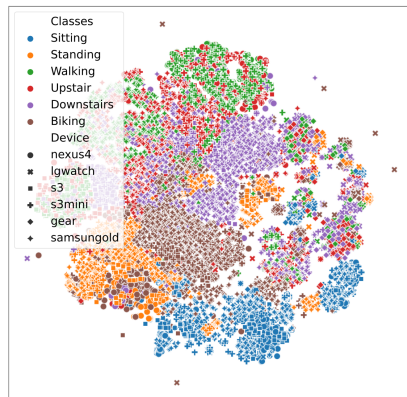


Figure 7: CNN HHAR

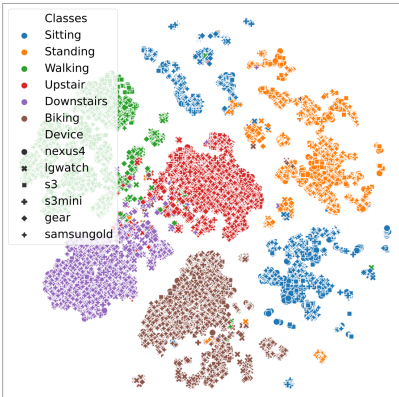


Figure 8: HART HHAR

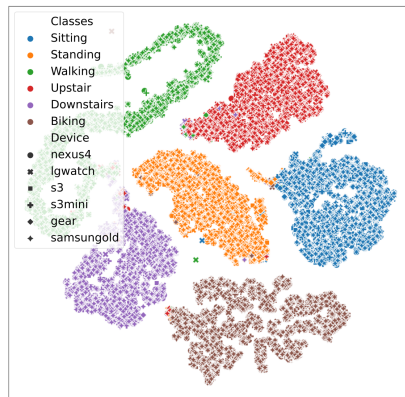


Figure 9: MobileHART (XS) HHAR

Table 5: Performance with unseen positions and devices on RealWorld & HHAR

Architecture	RealWorld							HHAR					
	Chest	Forearm	Head	Shin	Thigh	Upperarm	Waist	S.Gear	LG.Watch	Nexus4	S3	S3 Mini	S+
CNN	67.09	37.19	47.80	45.50	51.76	56.83	45.78	65.58	59.88	96.33	85.70	91.46	78.28
CNN-LSTM	65.11	25.78	42.05	39.21	47.86	51.68	34.42	57.62	62.24	94.59	76.35	90.71	84.33
HART	54.15	26.32	42.71	38.29	45.92	48.46	39.35	63.62	60.62	95.88	93.51	93.83	92.30
MobileHART (XS)	74.58	49.76	61.48	47.43	54.75	69.34	50.62	81.47	81.37	98.32	91.41	97.25	94.72

around all other activities. The representations on the HHAR dataset, on the other hand, show better separation between classes, except for the ‘Walking’ and ‘Upstairs’ activities which are often shown mixed together. Furthermore, the activities are not individually clustered, and the representation of devices are segregated.

Figures 5 and 8 show the representations generated by HART also on RW and HHAR. Comparing the representations of HART to those of the CNN, we observe a much better separation of classes. On the RW dataset, ‘Downstairs’ and ‘Upstairs’ activities are now separated and well clustered. However, the ‘Sitting’ and ‘Standing’ activities are still intertwined, and the ‘Lying’ activities remain at the edge of all activities without their own cluster. Conversely, the embeddings of HART on the HHAR dataset show a significant improvement in the clustering of activities, except for the ‘Sitting’ activity, where the representations are broken into two well-separated clusters.

MobileHART representations (Figures 6 and 9) are qualitatively best. We can observe a clear separation between classes on RW and HHAR. The representations from different positions or devices are respectively well clustered together with the activities. Specifically, on the RW dataset, the ‘Lying’ activity spiraling around other activities in the previous two model representations is now well-formed into a single cluster. On the HHAR dataset, the ‘Sitting’ activity is now grouped into a single cluster.

A fundamental need of daily-life HAR applications is the ability to work without the constraint of a specific device-location placement or a specific sensing device system. The effect of positions on the performances of HAR models has been subject to several studies [59, 60]. For HAR on mobile devices, the aim is to obtain a model agnostic to the device’s position or the device’s brand. To evaluate to which extent the models are robust to such domain shift, we present a quantitative evaluation where the HAR models are used to infer activities from different situations that have not been seen at training time.

With the RealWorld dataset, 1 position out of all 7 positions was left out as a test set, and training was performed on the remaining 6 positions. This process was repeated for all other positions. With the HHAR dataset, we follow the same process except that one model of the device was left out for testing, and the remaining devices were used for training. The process was repeated for all 6 devices model. The F-scores of the CNN, CNN-LSTM, HART, and MobileHART (XS) in this evaluation set-up are shown in Table 5.

The results on the RealWorld dataset (Tab. 5 left) show that inferring activity from a mobile device position that was not represented in the training data is very challenging. Activity recognition on the ‘Forearm’ and ‘Shin’ positions is especially difficult since no model can obtain an F-score above 50%. Overall, the CNN-LSTM and HART models obtain the lowest F-score across all positions. The CNN-LSTM model has the lowest performance when evaluating the ‘Forearm’ position with an F-score of 25.78%. The CNN model appears more robust than the previous two approaches

Table 6: Ablation of HART on UCI

Architecture	F-Score (\uparrow)	Parameters (\downarrow)	FLOPS (\downarrow)
ViT	93.66	3,783,238	17,069,949
ViT + LiteConv	94.10	1,443,326	15,179,228
ViT + SW MSA	94.21	2,446,534	15,091,292
HART	94.49	1,445,918	15,212,636

by obtaining a 2% to 10% increase in F-score. MobileHART (XS) outperformed all other architectures in all body positions. The highest score on unseen positions was by MobileHART (XS) on the 'Chest' location. In addition, the performance gain between MobileHART and CNN can be nearly as high as 13.68% on the 'Head' position and as low as 1.93% on the 'Shin' position.

On the HHAR dataset, not having a device in the training data creates a lesser detrimental effect. As previously, CNN-LSTM has the lowest performance with an F-score of 57.62% on the Samsung Gear Watch. Here HART and CNN obtained competitive scores. However, except for the Samsung S3 device, where HART had an F-score of 93.51%, MobileHART (XS) again vastly outperformed other models with a score as high as 98.32% on the Nexus 4 device. We note here that the Samsung Gear and LG Watch were smartwatches positioned on the wrist, while the other phones were conveyed in a hip-mounted pouch. Hence, for these cases, the models have to address the challenges of both system and statistical heterogeneity.

Our results here show that statistical heterogeneity, e.g., the different on-body position of sensors, has more impact on the performance of the models than system heterogeneity, e.g., different sensing device systems. Regarding model architectures, our models HART and MobileHART are in-line with the literature [9], where we require both the spatial (or temporal in our case) capability that CNNs provide and the input-adaptive weighting with global processing that the attention-based model provides. This was demonstrated by the performance of MobileHART (XS), which on the whole, was able to learn a much more coherent representation than other models and was more robust to system and statistical heterogeneity.

6 Architecture Evaluation

6.1 Ablation

Ablation experiments of HART are reported in Table 6, where the results show that the two designs can both improve over ViT in terms of F-score, Parameters, and FLOPS. LiteConv allowed the model to significantly decrease its parameter by more than half with a 0.44% increase in F-score. At the same time, the sensor-wise design gave a more robust increase in performance (0.55% increase over ViT) and reduced the models to the least number of FLOPS against other designs.

6.2 Scaling Study

We conducted a scaling study of ViT, HART, and HART_{OneMSA}, where we implemented the full 12-layered ViT model on the UCI dataset with the 'Small' configuration (embedding size of $d = 384$, attention headcount of $H = 6$) and 'Base' configuration (embedding size of $d = 768$, attention headcount of $H = 12$). The outcome of the models, reported in table 7, shows that the bigger the model (Big projection size, large attention head, and layer count), the larger impact HART design has on reducing parameters count. The HART_{OneMSA}^{Base} design reduced the parameter count from ViT^{Base} by 7.30 times and reduced the FLOPS count by nearly 60 million. Furthermore, our results showed that using the 'Base' configuration was too large for the model to converge, although using the original 'Small' configuration allowed us to push further the performance of HART on UCI (0.79% above our 6-layered 'Tiny' configuration).

6.3 Varying Sensors

Here we show the results of HART beyond the usage of only the accelerometer and gyroscope sensors and determine if the model is able to scale with more sensors. We thus evaluate HART on the MotionSense dataset when we add a magnetometer that senses magnetic field intensities. We note that the embedding dimension d is not increased with more sensors. Using the same embedding dimension d size of 192, the partitioning of the embeddings for 3 sensors is

Table 7: Scaling Study of HART and ViT on UCI

Architecture	F-Score (\uparrow)	Parameters (\downarrow)	FLOPS (\downarrow)
ViT ^{Base}	92.95	369,332,998	518,646,935
HART ^{Base}	94.86	71,857,062	462,246,524
HART ^{Base} _{OneMSA}	94.87	50,538,150	461,297,276
ViT ^{Small}	93.53	50,107,270	130,933,679
HART ^{Small}	95.28	12,886,422	116,606,588
HART ^{Small} _{OneMSA}	94.27	10,210,326	116,353,148

Table 8: HART with different sensors on MotionSense

Sensors	F-Score
Accelerometer, Gyroscope	98.13
Accelerometer, Magnetometer	98.21
Accelerometer, Gyroscope, Magnetometer	99.00

specifically as so: 96 for LightConv ($d/2$) and 32 each for all three sensors MSA ($d/6$). We further exemplify that with four sensors, the embedding size would be further reduced to 24 for each sensor ($d/8$).

The findings are presented in table 8, which shows that HART can adapt with an additional sensor where we see a 1.00% gain when the magnetometer is added on top of the Accelerometer and Gyroscope. Additionally, we trained different combinations of sensors where we used accelerometer and magnetometer, which showed a slight improvement in results (0.07% gain over accelerometer and gyroscope). In HAR on mobile devices, using fewer sensors allows developers an immense degree of freedom in terms of cost and product choices. The results here thus hint that only two sensors may be sufficient for HAR, as using the magnetometer and other less common sensors adds little performance gains [44].

7 Conclusion & Future Works

In this study, we present Human Activity Recognition Transformer (HART), an original Human Activity Recognition (HAR) approach for mobile devices using a Transformer-based model. The model is based on the successful transformer-based model in the vision domain (ViT). However, HART is specifically adapted for the HAR domain on mobile devices since we made its architecture lightweight and sensor-wise. With such architecture, HART was able to outperform the adapted ViT in all our benchmarks while using far less computation and memory footprint.

The HART architecture was extended to MobileViT, which devised MobileHART. This architecture, also compared againsts classical lightweight CNN and CNN-LSTM, outperformed all state-of-the-art models on several datasets. Also, thanks to the efficient light attention-based mechanism and Convolutional layers, the model exhibits excellent properties regarding model size and the number of operations. Moreover, we conducted several experiments to understand the remarkable ability of MobileHART better. The representation space analysis showed that HART could construct a more efficient embedding space than other models. Likewise, MobileHART shows the most excellent robustness in handling domain shifts, whether unseen mobile placement positions or unseen device brands, showing that MobileHART can generalize well to deal with unseen situations. Furthermore, the real device’s evaluation showed that MobileHART could run in real-time with negligible memory consumption.

Our work has demonstrated that HART can indeed run on mobile devices, exhibiting superior performances with lower cost as compared to other transformer-based approaches during inference. We thus set out to further study the on-device learning potential in the form of federated learning [61] with HART. Other studies have shown that it is indeed possible to integrate transformers into a collaborative learning ecosystem [62, 63], and we would extend our future work, in particular, to handle heterogeneity within a federated learning environment.

8 Acknowledgement

This work has been partially funded by Naval Group, France and by MIAI@Grenoble Alpes (ANR-19-P3IA-0003) funded by the French program Investissement d’avenir. This work was also granted access to the HPC resources of IDRIS under the allocation 2022-AD011013233 made by GENCI.

References

- [1] Mark Weiser. The computer for the 21 st century. *Scientific american*, 265(3):94–105, 1991.
- [2] C. Becker, C. Julien, P. Lalanda, and F. Zambonelli. Pervasive computing middleware: current trends and emerging challenges. *CCF Transactions on Pervasive Computing and Interaction*, vol. 1, 2019.
- [3] Rex Liu, Albara Ah Ramli, Huanle Zhang, Erik Henricson, and Xin Liu. An overview of human activity recognition using wearable sensors: Healthcare and artificial intelligence. In Bedir Tekinerdogan, Yingwei Wang, and Liang-Jie Zhang, editors, *Internet of Things – ICIOT 2021*, pages 1–14, Cham, 2022. Springer International Publishing.
- [4] Daniel Roggen, Gerhard Tröster, Paul Lukowicz, Alois Ferscha, José del R Millán, and Ricardo Chavarriaga. Opportunistic human activity and context recognition. *Computer*, 46(2):36–45, 2012.
- [5] Fuqiang Gu, Mu-Huan Chung, Mark Chignell, Shahrokh Valaee, Baoding Zhou, and Xue Liu. A survey on deep learning for human activity recognition. *ACM Computing Surveys (CSUR)*, 54(8):1–34, 2021.
- [6] Sruvan Kumar Challa, Akhilesh Kumar, and Vijay Bhaskar Semwal. A multibranch cnn-bilstm model for human activity recognition using wearable sensor data. *The Visual Computer*, pages 1–15, 2021.
- [7] Tian Li, Anit Kumar Sahu, Manzil Zaheer, Maziar Sanjabi, Ameet Talwalkar, and Virginia Smith. Federated optimization in heterogeneous networks. *Proceedings of Machine Learning and Systems*, 2:429–450, 2020.
- [8] Alexey Dosovitskiy, Lucas Beyer, Alexander Kolesnikov, Dirk Weissenborn, Xiaohua Zhai, Thomas Unterthiner, Mostafa Dehghani, Matthias Minderer, Georg Heigold, Sylvain Gelly, Jakob Uszkoreit, and Neil Houlsby. An image is worth 16x16 words: Transformers for image recognition at scale. In *International Conference on Learning Representations*, 2021.
- [9] Sachin Mehta and Mohammad Rastegari. Mobilevit: Light-weight, general-purpose, and mobile-friendly vision transformer. In *International Conference on Learning Representations*, 2022.
- [10] Vishakha V Vyas, KH Walse, and RV Dharaskar. A survey on human activity recognition using smartphone. *International Journal*, 5(3), 2017.
- [11] Kaixuan Chen, Dalin Zhang, Lina Yao, Bin Guo, Zhiwen Yu, and Yunhao Liu. Deep learning for sensor-based human activity recognition: Overview, challenges, and opportunities. *ACM Computing Surveys (CSUR)*, 54(4):1–40, 2021.
- [12] Wenchao Jiang and Zhaozheng Yin. Human activity recognition using wearable sensors by deep convolutional neural networks. In *Proceedings of the 23rd ACM International Conference on Multimedia*, MM ’15, page 1307–1310, New York, NY, USA, 2015. Association for Computing Machinery.
- [13] Yuanqing Zheng, Guobin Shen, Liqun Li, Chunshui Zhao, Mo Li, and Feng Zhao. Travi-navi: Self-deployable indoor navigation system. *IEEE/ACM Transactions on Networking*, 25(5):2655–2669, 2017.
- [14] E Ramanujam, Thinakaran Perumal, and S Padmavathi. Human activity recognition with smartphone and wearable sensors using deep learning techniques: A review. *IEEE Sensors Journal*, 2021.
- [15] Andrey D. Ignatov. Real-time human activity recognition from accelerometer data using convolutional neural networks. *Appl. Soft Comput.*, 62:915–922, 2018.
- [16] Bandar Almaslakh, Abdel Monim Artoli, and Jalal Al-Muhtadi. A robust deep learning approach for position-independent smartphone-based human activity recognition. *Sensors*, 18(11), 2018.
- [17] Ashish Vaswani, Noam Shazeer, Niki Parmar, Jakob Uszkoreit, Llion Jones, Aidan N Gomez, Łukasz Kaiser, and Illia Polosukhin. Attention is all you need. In I. Guyon, U. Von Luxburg, S. Bengio, H. Wallach, R. Fergus, S. Vishwanathan, and R. Garnett, editors, *Advances in Neural Information Processing Systems*, volume 30. Curran Associates, Inc., 2017.
- [18] Saif Mahmud, M Tanjid Hasan Tonmoy, Kishor Kumar Bhaumik, A K M Mahbubur Rahman, M Ashraf Amin, Mohammad Shoyaib, Muhammad Asif Hossain Khan, and Amin Ahsan Ali. Human activity recognition from wearable sensor data using self-attention, 2020.
- [19] Carlos Betancourt, Wen-Hui Chen, and Chi-Wei Kuan. Self-attention networks for human activity recognition using wearable devices. In *2020 IEEE International Conference on Systems, Man, and Cybernetics (SMC)*, pages 1194–1199, 2020.
- [20] Yoli Shavit and Itzik Klein. Boosting inertial-based human activity recognition with transformers. *IEEE Access*, 9:53540–53547, 2021.

- [21] Iveta Dirgová Luptáková, Martin Kubovčík, and Jiří Pospíchal. Wearable sensor-based human activity recognition with transformer model. *Sensors*, 22(5), 2022.
- [22] Huatao Xu, Pengfei Zhou, Rui Tan, Mo Li, and Guobin Shen. Limu-bert: Unleashing the potential of unlabeled data for imu sensing applications. In *Proceedings of the 19th ACM Conference on Embedded Networked Sensor Systems*, SenSys '21, page 220–233, New York, NY, USA, 2021. Association for Computing Machinery.
- [23] Salman Khan, Muzammal Naseer, Munawar Hayat, Syed Waqas Zamir, Fahad Shahbaz Khan, and Mubarak Shah. Transformers in vision: A survey. *ACM Computing Surveys (CSUR)*, 2021.
- [24] Yangtao Wang, Xi Shen, Shell Xu Hu, Yuan Yuan, James L. Crowley, and Dominique Vaufreydaz. Self-supervised transformers for unsupervised object discovery using normalized cut. In *Conference on Computer Vision and Pattern Recognition*, New Orleans, LA, USA, June 2022.
- [25] Mathilde Caron, Hugo Touvron, Ishan Misra, Hervé Jégou, Julien Mairal, Piotr Bojanowski, and Armand Joulin. Emerging properties in self-supervised vision transformers. In *Proceedings of the IEEE/CVF International Conference on Computer Vision*, pages 9650–9660, 2021.
- [26] Kaiming He, Xinlei Chen, Saining Xie, Yanghao Li, Piotr Dollár, and Ross Girshick. Masked autoencoders are scalable vision learners. *arXiv preprint arXiv:2111.06377*, 2021.
- [27] Xinlei Chen, Saining Xie, and Kaiming He. An empirical study of training self-supervised vision transformers. In *Proceedings of the IEEE/CVF International Conference on Computer Vision*, pages 9640–9649, 2021.
- [28] Jinnian Zhang, Houwen Peng, Kan Wu, Mengchen Liu, Bin Xiao, Jianlong Fu, and Lu Yuan. Minivit: Compressing vision transformers with weight multiplexing. *arXiv preprint arXiv:2204.07154*, 2022.
- [29] Ze Liu, Yutong Lin, Yue Cao, Han Hu, Yixuan Wei, Zheng Zhang, Stephen Lin, and Baining Guo. Swin transformer: Hierarchical vision transformer using shifted windows. In *Proceedings of the IEEE/CVF International Conference on Computer Vision*, pages 10012–10022, 2021.
- [30] Yinpeng Chen, Xiyang Dai, Dongdong Chen, Mengchen Liu, Xiaoyi Dong, Lu Yuan, and Zicheng Liu. Mobileformer: Bridging mobilenet and transformer. *arXiv preprint arXiv:2108.05895*, 2021.
- [31] Mark Sandler, Andrew Howard, Menglong Zhu, Andrey Zhmoginov, and Liang-Chieh Chen. Mobilenetv2: Inverted residuals and linear bottlenecks. In *Proceedings of the IEEE conference on computer vision and pattern recognition*, pages 4510–4520, 2018.
- [32] Andrew G Howard, Menglong Zhu, Bo Chen, Dmitry Kalenichenko, Weijun Wang, Tobias Weyand, Marco Andreetto, and Hartwig Adam. Mobilenets: Efficient convolutional neural networks for mobile vision applications. *arXiv preprint arXiv:1704.04861*, 2017.
- [33] Hugo Touvron, Matthieu Cord, Matthijs Douze, Francisco Massa, Alexandre Sablayrolles, and Hervé Jégou. Training data-efficient image transformers & distillation through attention. In *International Conference on Machine Learning*, pages 10347–10357. PMLR, 2021.
- [34] Kaiming He, Xiangyu Zhang, Shaoqing Ren, and Jian Sun. Deep residual learning for image recognition. In *Proceedings of the IEEE conference on computer vision and pattern recognition*, pages 770–778, 2016.
- [35] Zhanghao Wu*, Zhijian Liu*, Ji Lin, Yujun Lin, and Song Han. Lite transformer with long-short range attention. In *International Conference on Learning Representations (ICLR)*, 2020.
- [36] Felix Wu, Angela Fan, Alexei Baevski, Yann N Dauphin, and Michael Auli. Pay less attention with lightweight and dynamic convolutions. *arXiv preprint arXiv:1901.10430*, 2019.
- [37] Peter Battaglia, Jessica Blake Chandler Hamrick, Victor Bapst, Alvaro Sanchez, Vinicius Zambaldi, Mateusz Malinowski, Andrea Tacchetti, David Raposo, Adam Santoro, Ryan Faulkner, Caglar Gulcehre, Francis Song, Andy Ballard, Justin Gilmer, George E. Dahl, Ashish Vaswani, Kelsey Allen, Charles Nash, Victoria Jayne Langston, Chris Dyer, Nicolas Heess, Daan Wierstra, Pushmeet Kohli, Matt Botvinick, Oriol Vinyals, Yujia Li, and Razvan Pascanu. Relational inductive biases, deep learning, and graph networks. *arXiv*, 2018.
- [38] Davide Anguita, Alessandro Ghio, Luca Oneto, Xavier Parra, and Jorge Luis Reyes-Ortiz. A public domain dataset for human activity recognition using smartphones. In *21st European Symposium on Artificial Neural Networks, ESANN 2013, Bruges, Belgium, April 24-26, 2013*, 2013.
- [39] Mohammad Malekzadeh, Richard G. Clegg, Andrea Cavallaro, and Hamed Haddadi. Protecting sensory data against sensitive inferences. In *Proceedings of the 1st Workshop on Privacy by Design in Distributed Systems*, W-P2DS'18, pages 2:1–2:6, New York, NY, USA, 2018. ACM.
- [40] Chi Ian Tang, Ignacio Perez-Pozuelo, Dimitris Spathis, and Cecilia Mascolo. Exploring contrastive learning in human activity recognition for healthcare. *arXiv preprint arXiv:2011.11542*, 2020.

- [41] Allan Stisen, Henrik Blunck, Sourav Bhattacharya, Thor Siiger Prentow, Mikkel Baun Kjærgaard, Anind Dey, Tobias Sonne, and Mads Møller Jensen. Smart devices are different: Assessing and mitigating mobile sensing heterogeneities for activity recognition. In *Proceedings of the 13th ACM Conference on Embedded Networked Sensor Systems*, page 127–140, New York, NY, USA, 2015.
- [42] T. Szytler and H. Stuckenschmidt. On-body localization of wearable devices: An investigation of position-aware activity recognition. In *2016 IEEE International Conference on Pervasive Computing and Communications (PerCom)*, pages 1–9, 2016.
- [43] Hristijan Gjoreski, Mathias Ciliberto, Lin Wang, Francisco Javier Ordonez Morales, Sami Mekki, Stefan Valentin, and Daniel Roggen. The university of sussex-huawei locomotion and transportation dataset for multimodal analytics with mobile devices. *IEEE Access*, 6:42592–42604, 2018.
- [44] Wesllen Sousa Lima, Eduardo Souto, Khalil El-Khatib, Roozbeh Jalali, and João Gama. Human activity recognition using inertial sensors in a smartphone: An overview. *Sensors*, 19:3213, 07 2019.
- [45] B. Almaslukh. An effective deep autoencoder approach for online smartphone-based human activity recognition. *International Journal of Computer Science and Network Security*, 17, 04 2017.
- [46] Xiaochun Yin, Zengguang Liu, Deyong Liu, and Xiaojun Ren. A novel cnn-based bi- lstm parallel model with attention mechanism for human activity recognition with noisy data. *Scientific Reports*, 12(1):1–11, 2022.
- [47] Martín Abadi, Ashish Agarwal, Paul Barham, Eugene Brevdo, Zhifeng Chen, Craig Citro, Greg S. Corrado, Andy Davis, Jeffrey Dean, Matthieu Devin, Sanjay Ghemawat, Ian Goodfellow, Andrew Harp, Geoffrey Irving, Michael Isard, Yangqing Jia, Rafal Jozefowicz, Lukasz Kaiser, Manjunath Kudlur, Josh Levenberg, Dandelion Mané, Rajat Monga, Sherry Moore, Derek Murray, Chris Olah, Mike Schuster, Jonathon Shlens, Benoit Steiner, Ilya Sutskever, Kunal Talwar, Paul Tucker, Vincent Vanhoucke, Vijay Vasudevan, Fernanda Viégas, Oriol Vinyals, Pete Warden, Martin Wattenberg, Martin Wicke, Yuan Yu, and Xiaoqiang Zheng. TensorFlow: Large-scale machine learning on heterogeneous systems, 2015. Software available from tensorflow.org.
- [48] Diederik P Kingma and Jimmy Ba. Adam: A method for stochastic optimization. *arXiv preprint arXiv:1412.6980*, 2014.
- [49] Ilya Loshchilov and Frank Hutter. Decoupled weight decay regularization. In *International Conference on Learning Representations*, 2019.
- [50] Ali Araabi and Christof Monz. Optimizing transformer for low-resource neural machine translation. In *Proceedings of the 28th International Conference on Computational Linguistics*, pages 3429–3435, Barcelona, Spain (Online), December 2020. International Committee on Computational Linguistics.
- [51] Gustav Larsson, Michael Maire, and Gregory Shakhnarovich. Fractalnet: Ultra-deep neural networks without residuals. In *ICLR*, 2017.
- [52] Gao Huang, Yu Sun, Zhuang Liu, Daniel Sedra, and Kilian Q Weinberger. Deep networks with stochastic depth. In *European conference on computer vision*, pages 646–661. Springer, 2016.
- [53] Prajit Ramachandran, Barret Zoph, and Quoc V. Le. Searching for activation functions, 2017.
- [54] Dan Hendrycks and Kevin Gimpel. Gaussian error linear units (gelus), 2016.
- [55] Sannara Ek, François Portet, Philippe Lalanda, and German Vega. Evaluation of federated learning aggregation algorithms: application to human activity recognition. In *Adjunct Proceedings of the 2020 ACM International Joint Conference on Pervasive and Ubiquitous Computing and Proceedings of the 2020 ACM International Symposium on Wearable Computers*, pages 638–643, 2020.
- [56] Ronald Mutegeki and Dong Seog Han. A cnn-lstm approach to human activity recognition. In *2020 International Conference on Artificial Intelligence in Information and Communication (ICAIIIC)*, pages 362–366, 2020.
- [57] Andreas Steiner, Alexander Kolesnikov, Xiaohua Zhai, Ross Wightman, Jakob Uszkoreit, and Lucas Beyer. How to train your vit? data, augmentation, and regularization in vision transformers, 2021.
- [58] Laurens Van der Maaten and Geoffrey Hinton. Visualizing data using t-sne. *Journal of machine learning research*, 9(11), 2008.
- [59] David Blachon, Doruk Cokun, and François Portet. On-line Context Aware Physical Activity Recognition from the Accelerometer and Audio Sensors of Smartphones. In *European Conference on Ambient Intelligence*, volume 8850 of *Ambient Intelligence*, pages 205–220, Eindhoven, Netherlands, 2014.
- [60] Timo Szytler, Heiner Stuckenschmidt, and Wolfgang Petrich. Position-aware activity recognition with wearable devices. *Pervasive and mobile computing*, 38:281–295, 2017.

- [61] Brendan McMahan, Eider Moore, Daniel Ramage, Seth Hampson, and Blaise Aguera y Arcas. Communication-efficient learning of deep networks from decentralized data. In *Artificial intelligence and statistics*, pages 1273–1282. PMLR, 2017.
- [62] Sangjoon Park, Gwanghyun Kim, Jeongsol Kim, Boah Kim, and Jong Chul Ye. Federated split task-agnostic vision transformer for COVID-19 CXR diagnosis. In A. Beygelzimer, Y. Dauphin, P. Liang, and J. Wortman Vaughan, editors, *Advances in Neural Information Processing Systems*, 2021.
- [63] Ali Raza, Kim Phuc Tran, Ludovic Koehl, Shujun Li, Xianyi Zeng, and Khaled Benzaidi. Lightweight transformer in federated setting for human activity recognition, 2021.